IJMS
Vol 51, No 8, August 2026

Original Article

Mulberrofuran G Induces Apoptosis and Cell Cycle Arrest Through Suppression of the JAK2/STAT3 Pathway by Direct JAK2 Inhibition and Reactive Oxygen Species Induction in the NCI-H460 Cell Line

Zhong-Rui Li[1], PhD; Yu Zheng[1], MD; Chao Han[2], PhD; Lei Wang[1], PhD

[1]Department of Rehabilitation, College of Acupuncture and Moxibustion and Massage Health Preservation and Rehabilitation, Nanjing University of Chinese Medicine, Nanjing, No. 138 Xianlin Avenue, Nanjing 210023, China; [2]State Key Laboratory of Natural Medicines, Jiangsu Key Laboratory of Bioactive Natural Product Research, School of Traditional Chinese Pharmacy, China Pharmaceutical University, 639 Longmian Avenue, Nanjing 211198, China

Correspondence:
Chao Han, PhD;
School of Traditional Chinese Pharmacy, China Pharmaceutical University, 639 Longmian Avenue, Postal code: 211198, Nanjing, China
Tel: +86 15952052127
Email: hanchao@cpu.edu.cn
Received: 01 November 2025
Revised: 31 January 2026
Accepted: 08 March 2026

What's Known

- Persistent activation of the JAK2/STAT3 signaling pathway contributes to tumor proliferation, survival, and therapy resistance in non-small cell lung cancer.
- Mulberrofuran G exhibits anticancer activity in several malignancies, but its mechanism and therapeutic relevance in large cell lung carcinoma remain unclear.

What's New

- This study provides the first evidence that mulberrofuran G directly inhibits Janus kinase 2 activity and suppresses JAK2/STAT3 signaling in large cell lung carcinoma cells.
- A hierarchical dual-hit mechanism involving reactive oxygen species induction and direct kinase inhibition is demonstrated, supported by *in vivo* zebrafish validation.

Abstract

Background: Large cell lung carcinoma (LCLC) is an aggressive non-small cell lung cancer subtype. Mulberrofuran G (MG) from *Morus alba* L. possesses pharmacological properties, but its anticancer mechanisms in LCLC remain unexplored. This study aimed to validate the antitumor activity of MG against NCI-H460 cells and elucidate its dual mechanism involving Janus kinase 2 (JAK2) inhibition and reactive oxygen species (ROS) induction.

Methods: This study was conducted at the Nanjing University of Chinese Medicine and China Pharmaceutical University, Nanjing, China, from 2023 to 2025. Cell viability was assessed via 3-(4,5-dimethylthiazol-2-yl)-2,5-diphenyltetrazolium bromide (MTT). Flow cytometry using annexin V-fluorescein isothiocyanate (FITC)/propidium iodide (PI), 2',7'-dichlorodihydrofluorescein diacetate (DCFH-DA), and 5,5',6,6'-tetrachloro-1,1',3,3'-tetraethylbenzimidazolylcarbocyanine iodide (JC-1) measured apoptosis, cell cycle, ROS, and mitochondrial membrane potential (MMP). Western blot analyzed p21, cyclin B1, caspases3/7/9, cleaved caspases3/7/9, poly(ADP-ribose) polymerase (PARP), cleaved PARP, JAK2, p-JAK2, signal transducer and activator of transcription 3 (STAT3) and p-STAT3. Interactions were confirmed via docking, cellular thermal shift assay, and ADP-Glo. *In vivo* efficacy was evaluated in zebrafish. Data analysis was performed using GraphPad Prism 8.0. Statistical significance was determined using Student's *t* test or one-way/two-way ANOVA followed by Tukey's *post hoc* test ($P<0.05$).

Results: MG suppressed proliferation (IC_{50}=9.90 μM), induced G2/M arrest, and triggered mitochondrial apoptosis. MG inhibited JAK2/STAT3 via direct kinase inhibition (IC_{50}=17.17 μM) and ROS-mediated suppression. N-acetylcysteine (NAC) reversed these effects. Zebrafish tumor growth decreased by 19.7% ($P<0.05$).

Conclusion: MG exerts anticancer effects against LCLC by inducing ROS accumulation and dual suppression of the JAK2/STAT3 pathway, highlighting its potential as a therapeutic candidate.

Please cite this article as: Li ZR, Zheng Y, Han C, Wang L. Mulberrofuran G Induces Apoptosis and Cell Cycle Arrest Through Suppression of the JAK2/STAT3 Pathway by Direct JAK2 Inhibition and Reactive Oxygen Species Induction in the NCI-H460 Cell Line. Iran J Med Sci. 2026;51(8):570-581. doi: 10.30476/ijms.2026.109449.4477.

Keywords ● Mulberrofuran G ● Reactive oxygen species ● Janus kinase 2 ● STAT3 Transcription factor

Introduction

Lung cancer remains a leading cause of cancer-related mortality worldwide, accounting for approximately 25% of all cancer deaths.[1] Among its subtypes, large cell lung carcinoma (LCLC)—a rare form of non-small cell lung cancer (NSCLC)—comprises 3–9% of cases and is characterized by aggressive growth, high invasiveness, and poor prognosis. Current treatments for LCLC include surgery, radiotherapy, chemotherapy, and immunotherapy. Chemotherapy remains the primary approach for advanced or inoperable cases. However, its efficacy is often limited by drug resistance and side effects. Therefore, developing more effective therapies and gaining a deeper understanding of the molecular drivers of LCLC progression are of clear clinical importance.

The JAK2/STAT3 signaling axis is a master regulator of several cancer hallmark processes, including cellular proliferation, survival, metastatic invasion, and blood vessel formation.[2] In LCLC, the activation frequency and molecular dynamics of this pathway remain less well characterized than in other NSCLC subtypes. Nevertheless, multiple lines of indirect evidence point toward its likely importance in this setting. For example, persistent JAK2/STAT3 activation has been observed across multiple NSCLC models and correlates strongly with aggressive tumor behaviors, such as resistance to apoptosis, unrestrained growth, and metastatic dissemination.[3] Because LCLC itself is recognized as an especially aggressive and poorly differentiated NSCLC variant, it is plausible that aberrant JAK2/STAT3 signaling similarly contributes to its malignant progression. This idea gains additional support from reports linking sustained JAK2/STAT3 activity to broader mechanisms of chemotherapy resistance and cancer stem celllike properties in lung cancer pathogenesis.[4] Consequently, therapeutic agents that can selectively disrupt this pathway represent a promising strategy for LCLC treatment, justifying dedicated research efforts to evaluate their efficacy within this specific disease context.

Natural products have long served as valuable sources of anticancer agents.[5] *Morus alba* L. (mulberry root bark), which has been used in traditional medicine for clearing lung heat, contains Diels-Alder adducts as its primary bioactive constituents.[6] Several of these adducts, such as Sanggenons C, G, and O, as well as chalcomoracin, have demonstrated notable antitumor properties.[7-11] Mulberrofuran G (MG), another adduct in this class, also exhibits a range of biological effects.[12-16] Previous studies have reported MG's antiproliferative activity in various cancer models: it induces apoptotic cell death in human leukemia HL60 cells through death-receptor and mitochondrial pathways, suppresses proliferation and migration in lung adenocarcinoma (A549) and squamous cell carcinoma (NCIH226) cells by directly inhibiting JAK2/STAT3 signaling.[17-19] However, the antitumor efficacy of MG in LCLC and its ability to selectively target this dysregulated pathway in this specific subtype remain largely unexplored. This gap limits our understanding of MG's potential as a targeted therapy for LCLC.

To address this gap, the present study aimed to systematically validate MG as a targeted inhibitor of the aberrantly activated JAK2/STAT3 pathway in LCLC using NCIH460 cells, and to elucidate its underlying anticancer mechanisms. Specifically, we investigated whether MG suppresses LCLC cell proliferation, induces cell cycle arrest, and promotes apoptosis by specifically abrogating aberrant JAK2/STAT3 activation, whether through direct interaction with JAK2 or via reactive oxygen species (ROS)-dependent pathway inhibition. Furthermore, we provide preliminary *in vivo* validation using a zebrafish xenograft model to bridge the gap between the *in vitro* findings and physiological relevance. This study provides a mechanistic foundation for advancing MG as a potential therapeutic agent for LCLC and expands the understanding of natural product-derived JAK2/STAT3 inhibitors targeting pathwayaddicted lung cancer subtypes.

Materials and Methods

This study was conducted at the Nanjing University of Chinese Medicine and China Pharmaceutical University, Nanjing, China, from September 2023 to August 2025. All experimental protocols were approved by the Institutional Ethical Review Committee of China Pharmaceutical University (Approval Code: YSL-20260211).

Materials and Reagents

MG was purchased from Push Bio-technology (Chengdu, China). Antibodies against caspases, cleaved caspases, PARP, cleaved PARP, p21, Cyclin B1, STAT3, p-STAT3, JAK2, p-JAK2, Bax, and Bcl-2 were from Cell Signaling Technology (Danvers, MA, USA), Abcam (Cambridge, UK), and EnoGene (Nanjing, China). NAC and MTT were obtained from Beyotime (Shanghai, China) and Solarbio (Beijing, China), respectively.

Cell Culture

The NCI-H460 human LCLC cell line was obtained from the Shanghai Institute of Biochemistry and Cell Biology (Shanghai, China). This cell line was selected because of its origin from a patient with large cell lung carcinoma and its documented constitutive activation of the STAT3 pathway, making it an appropriate model for this study.[20] Cells were cultured in Dulbecco's modified Eagle medium with 10% fetal bovine serum and 1% antibiotics at 37 °C, 5% CO_2.

Cell Viability and Proliferation

Cells were treated with MG (0-100 μM) for 24-72 h. Viability was assessed using the MTT assay. The concentration range was selected based on previous literature reporting IC_{50} for Diels-Alder adducts in the low micromolar range and preliminary screening experiments to ensure coverage of the effective dose.[17, 21] Proliferation was evaluated using CFDA-SE tracing, colony formation, and EdU assays.[10]

Flow Cytometric Analysis

Flow cytometry was employed to assess apoptosis, cell cycle distribution, mitochondrial membrane potential (MMP), and intracellular ROS levels. Specifically, apoptosis was determined using annexin V-FITC/PI double staining; the cell cycle was analyzed by PI staining; MMP was measured with 5,5',6,6'-tetrachloro-1,1',3,3'-tetraethylbenzimidazolylcarbocyanine iodide (JC-1) dye; and ROS generation was detected using the fluorescent probe DCFH-DA. All flow cytometry kits were procured from KeyGen Biotech (Nanjing, China). Samples were analyzed using a BD Accuri™ C6 flow cytometer (BD Biosciences, San Jose, CA, USA).

Western Blot Analysis

Protein extraction from NCI-H460 cells treated with MG for 48 hours was performed using the lysis buffer. After quantifying protein concentration via bicinchoninic acid assay, equal amounts (30-40 μg per lane) were separated by sodium dodecyl sulfate-polyacrylamide gel electrophoresis (SDS-PAGE) and transferred to nitrocellulose membranes. The membranes were blocked with 5% skim milk, incubated overnight with primary antibodies at 4 °C, and then with horseradish peroxidase-conjugated secondary antibody. Protein bands were visualized using an enhanced chemiluminescence detection kit (Tanon, Shanghai, China).

RNA-seq Analysis

Total RNA was extracted from cells treated with MG or DMSO. Sequencing libraries were generated using the NEBNext® Ultra™ RNA Library Prep Kit and sequenced on an Illumina NovaSeq platform (Illumina, San Diego, CA, USA). Clean reads were aligned to the reference genome using Hisat2. Differential expression analysis was performed using DESeq2. To control for multiple testing and minimize Type I errors, P values were adjusted using the Benjamini-Hochberg procedure. Genes with an adjusted P value<0.05 and |log2 fold change|≥1 were identified as differentially expressed genes (DEGs). Functional enrichment was analyzed via gene ontology (GO) and Kyoto Encyclopedia of Genes and Genomes (KEGG) pathways.

Molecular Docking

Molecular docking was performed using Molsoft ICM-Pro 3.9-4 (Molsoft L.L.C., San Diego, CA, USA). The crystal structure of JAK2 (PDB: 3LPB) was prepared by removing solvent, adding hydrogens, and optimizing residue states. The ligand (MG) was docked into the refined model, and binding affinities were evaluated with the internal scoring function.

Cellular Thermal Shift Assay

NCI-H460 cells were treated with 10 μM MG or a DMSO-treated control for 1 hour. After washing with cold PBS, cell pellets were resuspended in PBS with protease inhibitors and heated at graded temperatures. The samples then underwent three freeze-thaw cycles using liquid nitrogen to achieve complete lysis. Following centrifugation, soluble protein extracts were subjected to immunoblotting to detect JAK2 levels, with GAPDH serving as the loading control.

In Vitro JAK2 Kinase Activity Assay

To validate direct inhibition, the ADP-Glo™ Kinase Assay (Promega, Madison, WI, USA) was employed. Recombinant human JAK2 kinase (0.2 ng/μL) was preincubated with MG (varying concentrations) or DMSO for 5 min. The reaction was initiated by adding ATP (25 μM) and PolyE4Y1 substrate (0.2 μg/μL) and incubated for 60 min. ADP production was quantified by measuring luminescence on a PerkinElmer EnSight™ reader (PerkinElmer, Waltham, MA, USA). The percentage inhibition and IC_{50} were calculated using non-linear regression in GraphPad Prism 8.0 (GraphPad Software, San Diego, CA, USA).

Zebrafish Xenograft Model

Wild-type zebrafish (AB strain) larvae (48 hpf) were microinjected with DiI-labeled NCI-H460 cells (~200 cells/larva) into the yolk sac. Larvae were randomly allocated to control (0.1% DMSO)

or treatment (10 μM MG) groups (n=22/group) and incubated at 28 °C for 72 hours. During this 72-hour incubation period, larvae were maintained in E3 medium without exogenous feeding to ensure they remained within the non-protected early life stage classification. Tumor burden was quantified by measuring red fluorescence intensity using ImageJ (NIH, Bethesda, MD, USA). Upon completion of the experiment at 120 hpf, all larvae were immediately euthanized using an overdose of tricaine methanesulfonate (MS-222), strictly adhering to ethical guidelines for early-life stage zebrafish models.

Statistical Analysis

All experiments were conducted at least three times independently, and results were presented as mean±SD and were analyzed with GraphPad Prism 8.0. Statistical significance was assessed using Student's *t* test (for two groups) or one-way/two-way ANOVA followed by Tukey's test (for multiple comparisons). Differences were considered statistically significant for $P<0.05$.

Results

MG Inhibits Proliferation in NCI-H460 Cells

To evaluate the anti-proliferative activity of MG (figure 1A) in LCLC, NCI-H460 cells were exposed to increasing concentrations of MG for 24-72 hours. As shown in figure 1B, MG significantly suppressed cell growth in a dose- and time-dependent manner, with IC_{50} values of 20.65 μM (24 h), 9.90 μM (48 hours), and 7.39 μM (72 h). Colony formation was also markedly inhibited by MG in a concentration-dependent manner (figure 1C). Furthermore, CFDA-SE tracing revealed that MG reduced cell division, as indicated by the increased fluorescence intensity (figure 1D). The EdU incorporation assay confirmed the anti-proliferative effect, showing a notable decrease in EdU-positive cells upon MG treatment (figure 1E). Collectively, these results demonstrate that MG acts as a potent inhibitor of NCI-H460 cell proliferation.

MG Induces G2/M Phase Arrest and Mitochondrial-Mediated Apoptosis in NCI-H460 Cells

Because cell cycle arrest represents a key mechanism for inhibiting tumor growth, we first examined the effect of MG on cell cycle progression.[22] Flow cytometric analysis revealed that MG treatment led to a dose-dependent accumulation of cells in the G2/M phase (figure 2 A, C). The proportion of G2/M phase cells increased from 9.2% (control) to 13.6% (10 μM) and 26.8% (20 μM), while the percentages of cells in G0/G1 and S phases showed no significant change, indicating that G2/M arrest contributes to the antiproliferative effects of MG.

We next investigated whether apoptosis induction represents another mechanism underlying MG's anti-tumor effects. Annexin V-FITC/PI staining showed that MG treatment significantly increased apoptosis rates from 2.39% (control) to 18.51% (10 μM) and 31.47% (20 μM) (figure 2 B, D). Consistent with these findings, Western blot analysis demonstrated that MG dose-dependently enhanced the cleavage of caspase-3, caspase-9, and PARP (figure 2 E, F), confirming the activation of caspase-dependent apoptosis.

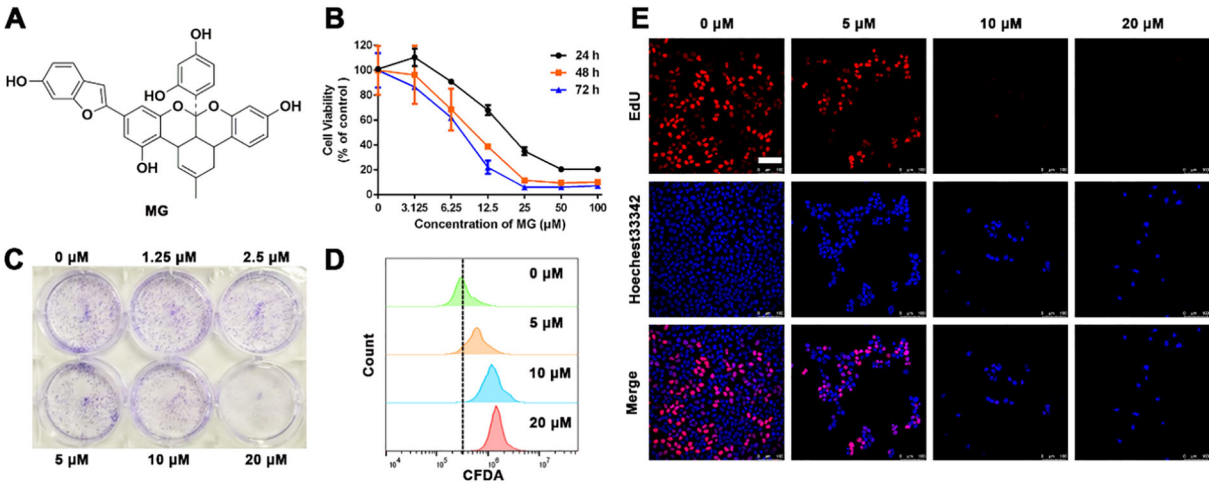

Figure 1: Mulberrofuran G inhibits proliferation in NCI-H460 cells. (A) Chemical structure of mulberrofuran G. (B) Cell viability after treatment with mulberrofuran G (0-100 μM) for 24-72 h was assessed by 3-(4,5-Dimethylthiazol-2-yl)-2,5-diphenyltetrazolium bromide assay. (C) Colony formation capacity following mulberrofuran G exposure for 8 days was examined. D) Following 48 hours of mulberrofuran G treatment, cell division was assessed by carboxyfluorescein diacetate, succinimidyl ester staining and flow cytometry. (E) After 48 hours of mulberrofuran G exposure, cell proliferation was evaluated using a 5-ethynyl-2'-deoxyuridine incorporation assay and visualized by confocal microscopy (scale bar: 100 μm). Data represent mean±SD from three independent experiments. MG: Mulberrofuran G; CFDA: Carboxyfluorescein diacetate; EdU: 5-ethynyl-2'-deoxyuridine

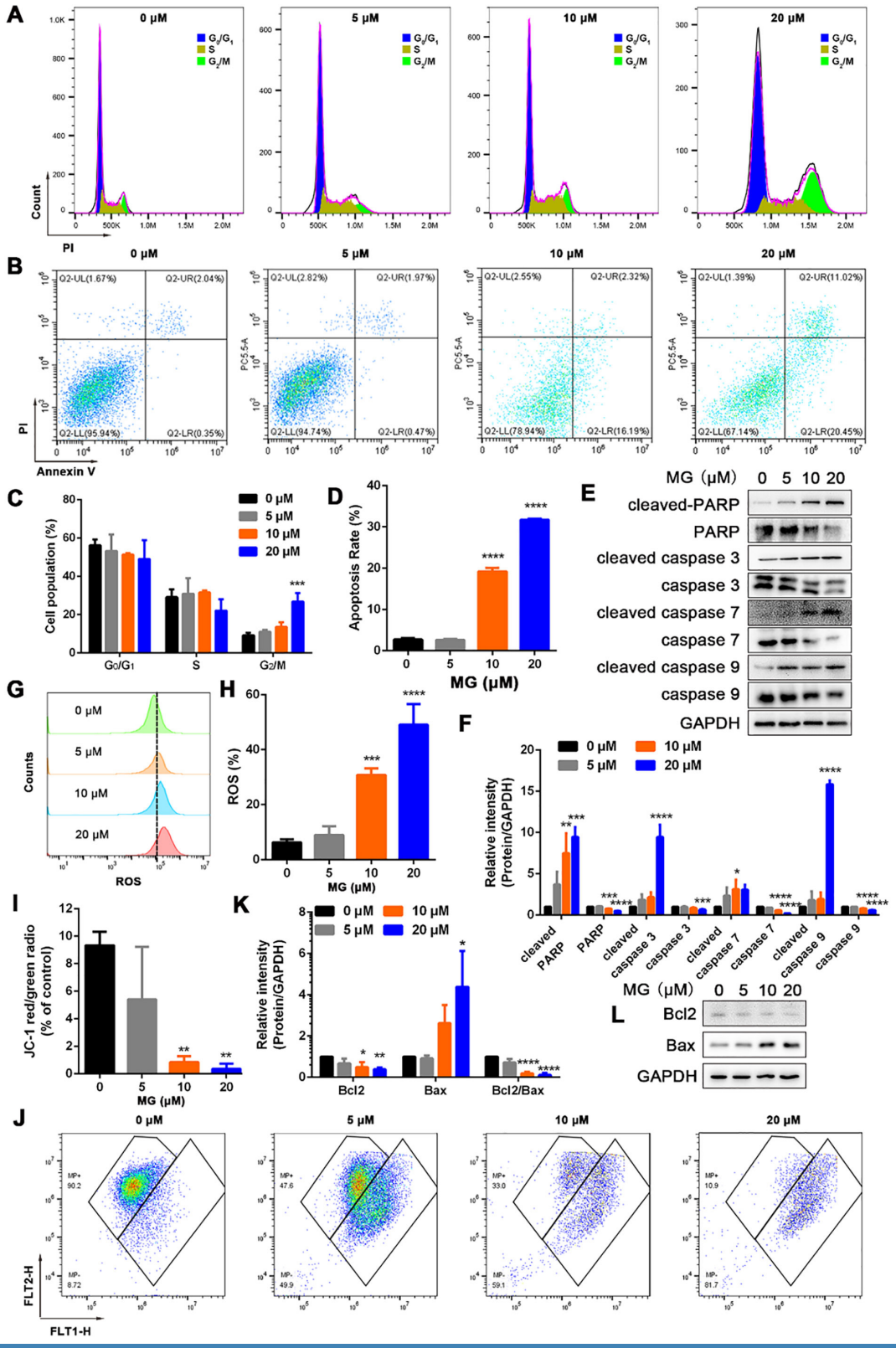

Figure 2: Mulberrofuran G triggers cell cycle arrest and mitochondrial apoptosis in NCI-H460 cells. Cells were treated with mulberrofuran G (0-20 μM) for 48 hours. (A) Cell cycle distribution analyzed by propidium iodide staining and flow cytometry. (B) Apoptosis rates determined by annexin V-fluorescein isothiocyanate/propidium iodide staining. (C-D) Quantitative analysis of (A) and (B), respectively. (E-F) Protein levels of apoptosis-related markers (cleaved poly(ADP-ribose) polymerase, caspase-3/7/9) assessed by Western blot. (G-H) Intracellular ROS levels measured using 2'7'-dichlorodihydrofluorescein diacetate. (I-J) Mitochondrial membrane potential (ΔΨm) evaluated by JC-1 staining. (K-L) Expression of Bcl-2 and Bax analyzed by Western blot. Data are represented as mean±SD of three independent experiments. *P<0.05, **P<0.01, ***P<0.001, ****P<0.0001 vs. control. PI: Propidium iodide; ROS: Reactive oxygen species; PARP: Poly(ADP-ribose) polymerase; GAPDH: Glyceraldehyde-3-phosphate dehydrogenase; JC-1: 5,5',6,6'-tetrachloro-1,1',3,3'-tetraethylbenzimidazolylcarbocyanine iodide

Given the close relationship between mitochondrial function and apoptosis induction, we further explored MG's effects on mitochondrial integrity.[23] JC-1 staining showed that MG significantly reduced mitochondrial membrane potential (MMP) in a concentration-dependent manner (figure 2 I, J). Concurrently, MG upregulated the pro-apoptotic protein Bax while downregulating the anti-apoptotic protein Bcl-2, resulting in a decreased Bcl-2/Bax ratio (figure 2 K, L) known to trigger caspase cascade activation.[24] Accompanying these mitochondrial alterations, MG treatment substantially increased intracellular ROS levels from 6.32% (control) to 30.8% (10 μM) and 49.1% (20 μM) as measured by DCFH-DA staining (figure 2 G, H). Collectively, these results demonstrate that MG induces apoptosis through the mitochondrial pathway, characterized by MMP collapse, altered Bcl-2 family protein expression, and ROS accumulation.

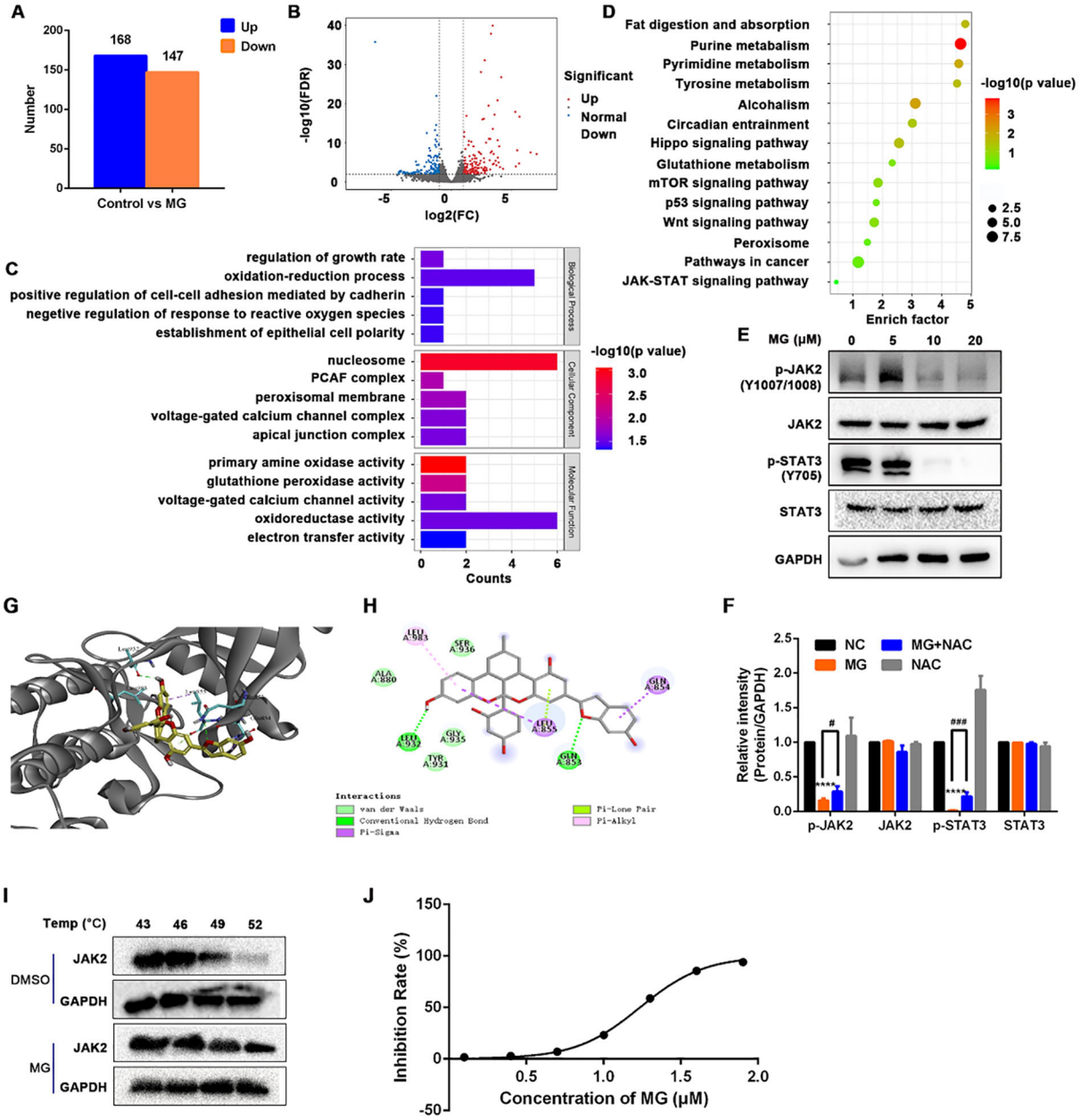

Figure 3: Mulberrofuran G disrupts redox homeostasis and inhibits Janus kinase 2/signal transducer and activator of transcription 3 signaling in NCI-H460 cells. (A) Statistics of differentially expressed genes. (B) Volcano plot of differentially expressed genes. (C) Gene ontology functional analysis of differentially expressed genes. (D) Kyoto Encyclopedia of Genes and Genomes pathway enrichment of differentially expressed genes. (E-F) Western blot analysis of Janus kinase 2/signaling transducer and activator of transcription 3 pathway proteins. (G-H) Molecular docking of mulberrofuran G into the Janus kinase 2 active site (PDB: 3LPB). (I) Cellular thermal shift assay showing mulberrofuran G-induced stabilization of Janus kinase 2. (J) Mulberrofuran G directly inhibits Janus kinase 2 kinase activity in a dose-dependent manner. Data represent mean±SD (n=3). ****P<0.0001 vs. control; #P<0.05, ###P<0.001, vs. mulberrofuran G alone. NC: Negative control; MG: Mulberrofuran G; JAK2: Janus kinase 2; STAT3: Signal transducer and activator of transcription 3; GAPDH: Glyceraldehyde-3-phosphate dehydrogenase

Unbiased Transcriptomic Analysis of MG-treated NCI-H460 Cells

To elucidate the antitumor mechanisms of MG, we conducted transcriptomic profiling of treated NCI-H460 cells. RNA-seq analysis identified 315 differentially expressed genes (168 upregulated, 147 downregulated; |FC|≥2, q<0.05) (figure 3A-B). Functional annotation revealed significant enrichment in redox processes, ROS regulation, and cell adhesion (GO analysis, figure 3C), while KEGG pathway analysis indicated involvement of peroxisome, glutathione metabolism, and cancer-related pathways including JAK-STAT, Wnt, and mTOR (figure 3D).

Based on transcriptomic analysis of JAK-STAT pathway involvement, we validated that MG substantially suppressed JAK2/STAT3 phosphorylation (figures 3E-F). To elucidate the binding mode of MG with its molecular target, molecular docking was performed using the crystal structure of the JAK2 tyrosine kinase domain (JH1) (PDB ID: 3LPB).

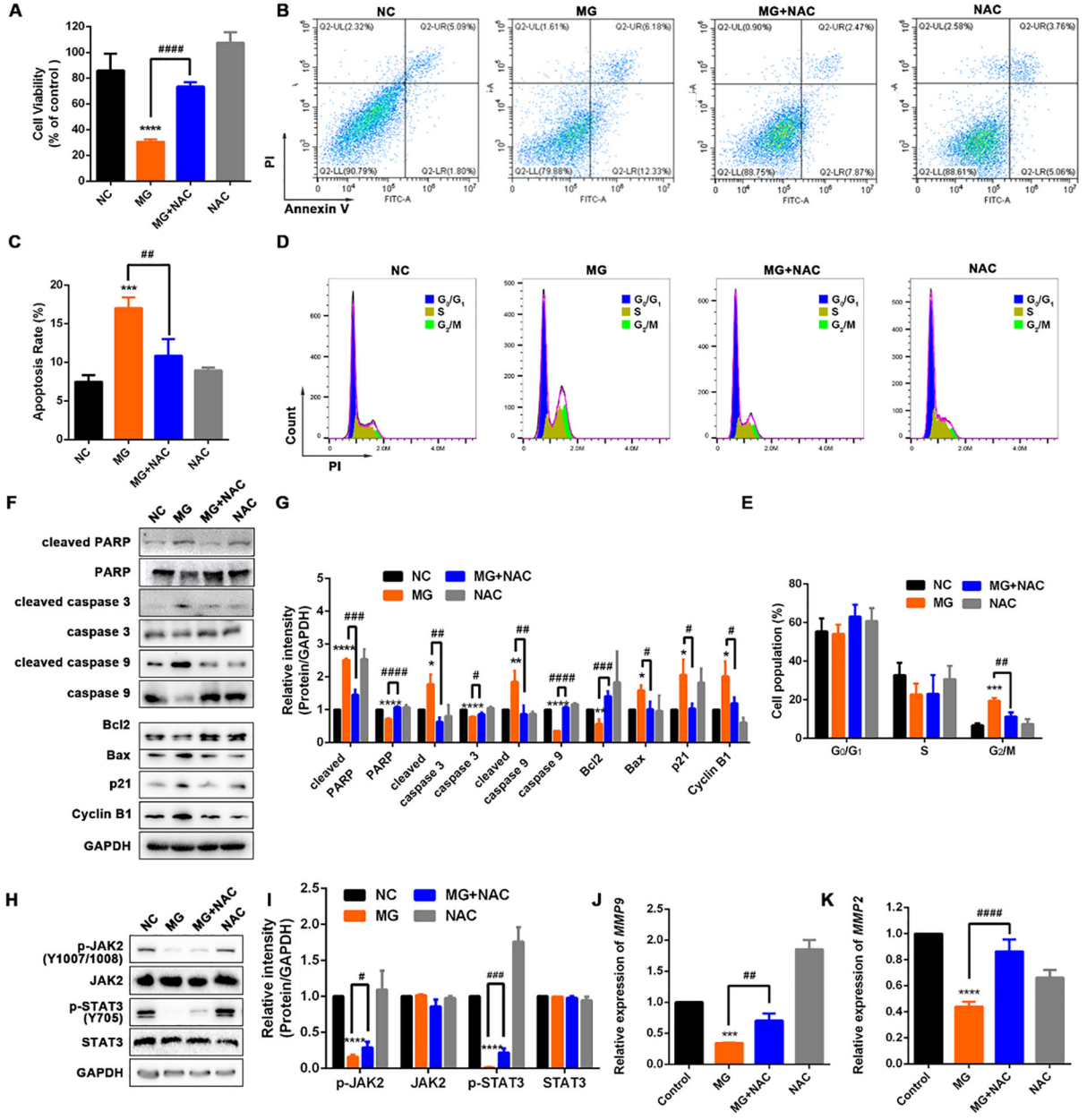

Figure 4: Reactive oxygen species scavenger N-acetyl-cysteine reverses mulberrofuran G-mediated effects in NCI-H460 cells. Cells were treated with mulberrofuran G (10 μM) alone or co-treated with N-acetyl-cysteine (5 mM) for 48 hours. (A) Cell viability. (B-C) Apoptosis analysis. (D-E) Cell cycle distribution. (F-G) Apoptosis and cell cycle-related protein expression. (H-I) Janus kinase 2/ signal transducer and activator of transcription 3 pathway protein levels. (J-K) mRNA expression of signal transducer and activator of transcription target genes, matrix metalloproteinase 9, and matrix metalloproteinase 2. Data represent mean±SD (n=3). *P<0.05, **P<0.01, ***P<0.001, ****P<0.0001 vs. control; #P<0.05, ##P<0.01, ###P<0.001, ####P<0.0001 vs. mulberrofuran G alone. NC: Negative control; MG: Mulberrofuran G; NAC: N-acetyl-cysteine; JAK2: Janus kinase 2; STAT3: Signal transducer and activator of transcription 3; *MMP9*: Matrix metalloproteinase 9; *MMP2*: Matrix metalloproteinase 2

The structural analysis revealed that MG fits securely into the ATP-binding pocket of JAK2, adopting a conformation that facilitates multi-point anchoring (figure 3 G-H). MG forms a hydrogen bond with the backbone of Leu932 located in the hinge region, a canonical interaction characteristic of ATP-competitive inhibitors that stabilizes the ligand within the catalytic cleft. Furthermore, MG engages in a specific hydrogen bond interaction with Gln853 in the N-lobe. Given that Gln853 is a non-conserved residue among JAK family members, this interaction may contribute to the specificity of MG for JAK2. Collectively, these computational findings support a mechanism where MG functions as a direct, Type I inhibitor of the JAK2 catalytic domain, thereby physically blocking ATP access and downstream signal transduction. Experimental validation via cellular thermal shift assay confirmed MG-induced JAK2 stabilization (figure 3I), collectively supporting JAK2 as a direct cellular target whose inhibition underlies MG's antitumor effects. To provide functional confirmation of this interaction, we performed a cell-free *in vitro* kinase assay. As shown in figure 3J, MG inhibited JAK2 enzymatic activity in a dose-dependent manner with an IC_{50} value of 17.17 μM. This finding demonstrates that MG directly inhibits JAK2 kinase.

ROS Scavenger Reverses the Effects of MG in NCI-H460 Cells

To confirm the essential role of ROS in MG's anticancer activity, we employed the antioxidant NAC. NAC significantly attenuated MG-induced cell death (figure 4A) and apoptosis. The apoptosis rate decreased from 18.51% (MG alone) to 10.34% (MG+NAC) (figure 4 B-C), consistent with reduced cleavage of caspase-3, caspase-9, and PARP (figure 4 F-G). Furthermore, NAC reversed the MG-mediated decrease in the Bcl-2/Bax ratio and alleviated G2/M phase arrest (figure 4 D-E). Notably, the MG-induced upregulation of p21 and Cyclin B1 was also reversed by NAC (figure 4 F-G), linking ROS-mediated oxidative stress directly to the cell cycle checkpoint activation.

At the signaling level, NAC restored the phosphorylation of JAK2 and STAT3 (figure 4H-I) and rescued the expression of STAT3 target genes matrix metalloproteinase 2 (*MMP2*) and matrix metalloproteinase 9 (*MMP9)*. These data collectively demonstrate that the anticancer effects of MG, including cell cycle arrest, apoptosis, and JAK2/STAT3 pathway suppression, are primarily mediated through ROS-dependent mechanisms.

MG Suppresses Tumor Proliferation in a Zebrafish Xenograft Model

As depicted in figure 5, MG treatment resulted in a significant reduction in tumor burden. Quantification of fluorescence intensity indicated a 19.7% inhibition of tumor cell proliferation compared to the negative control group ($P<0.05$, $n=22$). This provides robust *in vivo* evidence supporting the therapeutic potential of MG.

Discussion

In this study, we provide a comprehensive evaluation of the antitumor efficacy and underlying molecular mechanisms of MG in LCLC. Our results demonstrate that MG significantly inhibits the proliferation of NCI-H460 cells by inducing G2/M phase arrest and mitochondrial-mediated apoptosis. This tumor-suppressive effect is driven by a dual mechanism involving the sensitive induction of ROS-dependent oxidative stress and direct enzymatic inhibition of the oncogenic JAK2/STAT3 signaling pathway. These findings identify MG as a promising, naturally derived candidate for LCLC therapy.

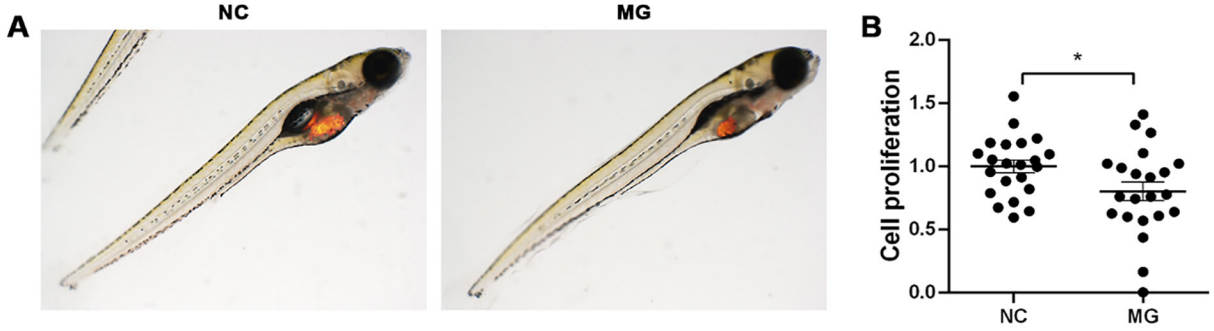

Figure 5: Mulberrofuran G suppresses tumor proliferation in a zebrafish xenograft model. (A) Representative fluorescent microscopy images of zebrafish larvae at 3 days post-inoculation (dpi) with fluorescently labeled NCI-H460 cells. Larvae were treated with mulberrofuran G or a negative control (0.1% DMSO) from 1 to 3 dpi. (B) Quantification of relative tumor fluorescence intensity, normalized to the control group. Mulberrofuran G treatment significantly reduced tumor cell proliferation by 19.7% compared to the control ($P<0.05$; $n=22$ larvae per group). Data are presented as mean±SD. Statistical analysis was performed using an unpaired two-tailed Student's *t* test. NC: Negative control; MG: Mulberrofuran G

MG, a benzofuran isolated from the root bark of *Morus alba*, exhibits diverse pharmacological activities. Although bioinformatic studies have suggested its potential as an anti-cancer agent and related compounds have shown activity in other lung cancer subtypes, MG's efficacy and mechanism in LCLC remain unclear.[24]

In the present study, we demonstrate that MG exerts potent antitumor activity against NCI-H460 cells by coordinately inducing oxidative stress and suppressing oncogenic JAK2/STAT3 signaling. Given that dysregulated cell-cycle progression is a hallmark of cancer, we investigated whether MG affects cell cycle progression.[25] MG significantly induced G2/M phase arrest, suggesting cell cycle blockade contributes to its anti-proliferative effect. This was mechanistically supported by the upregulation of p21 and cyclin B1, proteins critical for the G2/M transition.

MG also induced mitochondrial apoptosis, evidenced by increased annexin V-FITC/PI staining and activation of caspase-3, -7, -9, and PARP cleavage. We found MG reduced mitochondrial membrane potential (MMP) and decreased the Bcl-2/Bax ratio, indicating activation of mitochondrial apoptotic pathway.[26] While our data highlight the mitochondrial pathway as a primary driver, consistent with the observed caspase-9 activation and Bcl-2/Bax modulation, we cannot exclude the potential involvement of the extrinsic death receptor pathway, as MG has been reported to trigger both pathways in leukemia cells.[17] Future studies assessing caspase-8 activation would help clarify this broader regulatory network.

Given the susceptibility of cancer cells to oxidative stress, we examined ROS involvement. MG increased ROS levels in a dose-dependent manner.[27] Transcriptomic analysis confirmed MG disrupts redox homeostasis, highlighting enrichment in peroxisome, glutathione metabolism, and cancer-related pathways, including JAK-STAT. Further investigation revealed that MG directly inhibits JAK2. This finding, initially predicted by SwissTargetPrediction, was confirmed by molecular docking and cellular thermal shift assay, and conclusively validated by an *in vitro* kinase assay (IC_{50}=17.17 μM), collectively supporting JAK2 as a direct functional target of MG.

To confirm ROS dependency, we co-treated cells with NAC. The ROS scavenger significantly reversed MG-induced cytotoxicity and apoptosis, restored the Bcl-2/Bax ratio, and attenuated G2/M arrest. NAC also rescued MG-mediated suppression of p-JAK2, p-STAT3, and STAT3 target genes *MMP2/MMP9*, confirming that MG exerts its anti-LCLC effects, at least in part, through ROS-mediated suppression of the JAK2/STAT3 pathway. The discrepancy between the kinase assay IC_{50} (17.17 μM) and the effective cellular concentrations (<10 μM) suggests a hierarchical mechanism: ROS induction likely serves as the primary, highly sensitive trigger that broadly inhibits phosphatases or kinases via oxidation, while direct JAK2 binding provides a secondary, reinforcing blockade of the survival pathway.[28]

A major strength of this study lies in its multi-layered mechanistic validation, integrating transcriptomic profiling, biochemical assays, and in silico docking with *in vivo* zebrafish xenograft modeling. By identifying the dual-target action—ROS induction and direct JAK2 inhibition—this work highlights the potential value of simultaneously targeting multiple components against the JAK2/STAT3 oncogenic network. Furthermore, the use of cellular thermal shift assay and kinase assays provides robust evidence for JAK2 as a direct functional target of MG, offering a solid mechanistic foundation for its development as a targeted therapy.

Despite these strengths, this study utilized a single LCLC cell line (NCI-H460), which is a limitation for generalizing findings across the heterogeneity of lung cancer. However, the consistent results across transcriptomic, biochemical, and cellular assays, strengthened by the zebrafish *in vivo* validation, provide a solid mechanistic proof-of-concept. Future studies should expand to a panel of NSCLC cell lines and mammalian xenograft models to fully characterize the clinical potential of MG.

Conclusion

Collectively, our findings establish MG as a dual-mechanism antitumor agent that suppresses the progression of NCI-H460 cells through ROS-dependent signaling disruption and direct enzymatic inhibition of JAK2, thereby providing a mechanistic foundation for further *in vivo* validation and translational exploration.

Supporting these findings, preliminary *in vivo* evidence obtained from a zebrafish xenograft model substantiates the ability of MG to suppress tumor growth, effectively connecting mechanistic understanding with relevant physiological responses. To further harness the therapeutic promise of MG, subsequent research should concentrate on the following priority areas: (i) extending experimental validation to a broader spectrum of LCLC and NSCLC cell lines; (ii) performing systematic assessments of efficacy, safety, and

pharmacokinetic properties in murine tumor systems; and (iii) examining potential synergistic effects of MG in combination with established chemotherapy regimens or immune-modulating agents. Ultimately, translational evaluation of MG's bioavailability and pharmacokinetic profile will be indispensable for its progression toward clinical application.

Acknowledgment

We express our gratitude to all individuals and organizations that contributed to the research and preparation of this manuscript. This work was co-supported by the National Natural Science Foundation of China (82104359), the China Postdoctoral Science Foundation (2021M691647) and the Open Project of State Key Laboratory of Natural Medicines (SKLNMKF202207).

Authors' Contribution

ZhR.L: Conceptualization; data curation; formal analysis; funding acquisition; investigation; methodology; project administration; writing-original draft; and reviewing the manuscript; Y.Zh: Data curation; formal analysis; methodology; software; visualization and reviewing the manuscript; Ch.H: Conceptualization; supervision; validation; project administration; drafting and reviewing the manuscript; L.W: Conceptualization; resources; supervision; drafting and reviewing the manuscript; All authors have read and approved the final manuscript and agree to be accountable for all aspects of the work in ensuring that questions related to the accuracy or integrity of any part of the work are appropriately investigated and resolved.

Declaration of AI

For language polishing and refinement only, the authors utilized the DeepSeek AI model (created by DeepSeek Company). All scientific content, data analysis, interpretation, and conclusions remain the sole responsibility of the authors.

Conflict of Interest: None declared.

References

1 Siegel RL, Giaquinto AN, Jemal A. Cancer statistics, 2024. CA Cancer J Clin. 2024;74:12-49. doi: 10.3322/caac.21820. PubMed PMID: 38230766.
2 Johnson DE, O'Keefe RA, Grandis JR. Targeting the IL-6/JAK/STAT3 signalling axis in cancer. Nat Rev Clin Oncol. 2018;15:234-48. doi: 10.1038/nrclinonc.2018.8. PubMed PMID: 29405201; PubMed Central PMCID: PMC5858971.
3 Liu X, Chen B, You W, Xue S, Qin H, Jiang H. The membrane bile acid receptor TGR5 drives cell growth and migration via activation of the JAK2/STAT3 signaling pathway in non-small cell lung cancer. Cancer Lett. 2018;412:194-207. doi: 10.1016/j.canlet.2017.10.017. PubMed PMID: 29074425.
4 Mengie Ayele T, Tilahun Muche Z, Behaile Teklemariam A, Bogale Kassie A, Chekol Abebe E. Role of JAK2/STAT3 Signaling Pathway in the Tumorigenesis, Chemotherapy Resistance, and Treatment of Solid Tumors: A Systemic Review. J Inflamm Res. 2022;15:1349-64. doi: 10.2147/JIR.S353489. PubMed PMID: 35241923; PubMed Central PMCID: PMC8887966.
5 Song Z, Chen G, Chen CY. AI empowering traditional Chinese medicine? Chem Sci. 2024;15:16844-86. doi: 10.1039/d4sc04107k. PubMed PMID: 39355231; PubMed Central PMCID: PMC11440359.
6 Zeng XX, Gao DD, Zhang F. Cortex Mori Radicis[Morus Alba L. (Moraceae)] extract alleviates senescence via PI3K/Akt signaling in COPD fibroblasts. Phytomedicine. 2024;135:156004. doi: 10.1016/j.phymed.2024.156004. PubMed PMID: 39326135.
7 Sun W, Cai H, Zhang K, Cui H, Zhao E. Targeting MCL1 with Sanggenon C overcomes MCL1-driven adaptive chemoresistance via dysregulation of autophagy and endoplasmic reticulum stress in cervical cancer. Phytomedicine. 2024;133:155935. doi: 10.1016/j.phymed.2024.155935. PubMed PMID: 39126925.
8 Hu X, Li J, Yu L, Ifejola J, Guo Y, Zhang D, et al. Screening of anti-melanoma compounds from Morus alba L.: Sanggenon C promotes melanoma cell apoptosis by disrupting intracellular Ca(2+) homeostasis. J Ethnopharmacol. 2024;324:117759. doi: 10.1016/j.jep.2024.117759. PubMed PMID: 38219884.
9 Park JE, Jung JH, Lee HJ, Sim DY, Im E, Park WY, et al. Ribosomal protein L5 mediated inhibition of c-Myc is critically involved in sanggenon G induced apoptosis in non-small lung cancer cells. Phytother Res. 2021;35:1080-8. doi: 10.1002/ptr.6878. PubMed PMID: 32935429.
10 Li ZR, Ma T, Guo YJ, Hu B, Niu SH, Suo FZ, et al. Sanggenon O induced apoptosis of A549 cells is counterbalanced by protective

autophagy. Bioorg Chem. 2019;87:688-98. doi: 10.1016/j.bioorg.2019.03.072. PubMed PMID: 30953888.
11 Zhang SR, Zhang XC, Liang JF, Fang HM, Huang HX, Zhao YY, et al. Chalcomoracin inhibits cell proliferation and increases sensitivity to radiotherapy in human non-small cell lung cancer cells via inducing endoplasmic reticulum stress-mediated paraptosis. Acta Pharmacol Sin. 2020;41:825-34. doi: 10.1038/s41401-019-0351-4. PubMed PMID: 32066885; PubMed Central PMCID: PMC7470873.
12 Koirala P, Seong SH, Zhou Y, Shrestha S, Jung HA, Choi JS. Structure(-)Activity Relationship of the Tyrosinase Inhibitors Kuwanon G, Mulberrofuran G, and Albanol B from Morus Species: A Kinetics and Molecular Docking Study. Molecules. 2018;23. doi: 10.3390/molecules23061413. PubMed PMID: 29891812; PubMed Central PMCID: PMC6099663.
13 Kim YS, Kim B, Kwon EB, Chung HS, Choi JG. Mulberrofuran G, a Mulberry Component, Prevents SARS-CoV-2 Infection by Blocking the Interaction between SARS-CoV-2 Spike Protein S1 Receptor-Binding Domain and Human Angiotensin-Converting Enzyme 2 Receptor. Nutrients. 2022;14. doi: 10.3390/nu14194170. PubMed PMID: 36235822; PubMed Central PMCID: PMC9573737.
14 Karpinski TM, Ozarowski M, Silva PJ, Stasiewicz M, Alam R, Samad A. Discovery of Terpenes as Novel HCV NS5B Polymerase Inhibitors via Molecular Docking. Pathogens. 2023;12. doi: 10.3390/pathogens12060842. PubMed PMID: 37375532; PubMed Central PMCID: PMC10305183.
15 Tian LL, Bi YX, Zhang H. Structurally Diverse Stilbenoids as Potent alpha-Glucosidase Inhibitors with Antidiabetic Effect from Morus alba. J Agric Food Chem. 2024;72:17938-52. doi: 10.1021/acs.jafc.4c01681. PubMed PMID: 39092914.
16 Hong S, Kwon J, Kim DW, Lee HJ, Lee D, Mar W. Mulberrofuran G Protects Ischemic Injury-induced Cell Death via Inhibition of NOX4-mediated ROS Generation and ER Stress. Phytother Res. 2017;31:321-9. doi: 10.1002/ptr.5754. PubMed PMID: 27910195.
17 Luo SY, Zhu JY, Zou MF, Yin S, Tang GH. Mulberry Diels-Alder-type adducts: isolation, structure, bioactivity, and synthesis. Nat Prod Bioprospect. 2022;12:31. doi: 10.1007/s13659-022-00355-y. PubMed PMID: 36050566; PubMed Central PMCID: PMC9436459.
18 Liu XX, Zhu XY, Yu Z. Mulberrofuran G inhibits proliferation and migration by inactivating JAK2/STAT3 signaling in lung cancer cells. Bangladesh J Pharmacol. 2021;16:134-40. doi: 10.3329/bjp.v16i4.55198.
19 Pu H, Cao D, Zhou X, Li F, Wang L, Wang M. Isoprenylated Flavonoids and 2-Arylbenzofurans from the Root Bark of Morus alba L. and Their Cytotoxic Activity against HGC27 Cancer Cells. Molecules. 2023;29. doi: 10.3390/molecules29010030. PubMed PMID: 38202613; PubMed Central PMCID: PMC10779849.
20 Son DJ, Zheng J, Jung YY, Hwang CJ, Lee HP, Woo JR, et al. MMPP Attenuates Non-Small Cell Lung Cancer Growth by Inhibiting the STAT3 DNA-Binding Activity via Direct Binding to the STAT3 DNA-Binding Domain. Theranostics. 2017;7:4632-42. doi: 10.7150/thno.18630. PubMed PMID: 29158850; PubMed Central PMCID: PMC5695154.
21 Phan TN, Kim O, Ha MT, Hwangbo C, Min BS, Lee JH. Albanol B from Mulberries Exerts Anti-Cancer Effect through Mitochondria ROS Production in Lung Cancer Cells and Suppresses In Vivo Tumor Growth. Int J Mol Sci. 2020;21. doi: 10.3390/ijms21249502. PubMed PMID: 33327489; PubMed Central PMCID: PMC7764986.
22 Matthews HK, Bertoli C, de Bruin RAM. Cell cycle control in cancer. Nat Rev Mol Cell Biol. 2022;23:74-88. doi: 10.1038/s41580-021-00404-3. PubMed PMID: 34508254.
23 Abate M, Festa A, Falco M, Lombardi A, Luce A, Grimaldi A, et al. Mitochondria as playmakers of apoptosis, autophagy and senescence. Semin Cell Dev Biol. 2020;98:139-53. doi: 10.1016/j.semcdb.2019.05.022. PubMed PMID: 31154010.
24 Xia-Liang C. Bioinformatic analysis of mulberrofuran G: A potential anticancer activity agent. Lat Am J Pharm. 2019;38:518-22.
25 Rodencal J, Kim N, He A, Li VL, Lange M, He J, et al. Sensitization of cancer cells to ferroptosis coincident with cell cycle arrest. Cell Chem Biol. 2024;31:234-48 e13. doi: 10.1016/j.chembiol.2023.10.011. PubMed PMID: 37963466; PubMed Central PMCID: PMC10925838.
26 Dou R, Cai X, Ruan L, Zhang J, Rouzi A, Chen J, et al. Precision Nanomedicines: Targeting Hot Mitochondria in Cancer Cells. ACS Appl Bio Mater. 2022;5:4103-17. doi: 10.1021/acsabm.2c00641. PubMed PMID: 36066886.
27 Glorieux C, Liu S, Trachootham D, Huang P. Targeting ROS in cancer: rationale and strategies. Nat Rev Drug Discov. 2024;23:583-606. doi: 10.1038/s41573-024-00979-4.

PubMed PMID: 38982305.

28 Cao Y, Wang J, Tian H, Fu GH. Mitochondrial ROS accumulation inhibiting JAK2/STAT3 pathway is a critical modulator of CYT997-induced autophagy and apoptosis in gastric cancer. J Exp Clin Cancer Res. 2020;39:119. doi: 10.1186/s13046-020-01621-y. PubMed PMID: 32576206; PubMed Central PMCID: PMC7310559.